High-conductivity poly(3,4-ethylenedioxythiophene):poly(styrene sulfonate) film for use in ITO-free polymer solar cells

Yu-Sheng Hsiao,[a] Wha-Tzong Whang,*[a] Chih-Ping Chen[b] and Yi-Chun Chen[b]

Received 29th July 2008, Accepted 7th October 2008
First published as an Advance Article on the web 4th November 2008
DOI: 10.1039/b813079e

In this study, we devised a simple method to enhance the conductivity of poly(3,4-ethylenedioxythiophene)-poly(styrene-sulfonate) (PEDOT:PSS) films through spin-coating with various surface-modified compounds, and then applied this technique to the preparation of ITO-free polymer solar cells (PSCs). The electrical conductivity of PEDOT:PSS films can be increased by more than two order of magnitudes merely by spin-coating a compound containing one or more polar groups—such as ethanol, methoxyethanol, 1,2-dimethoxyethane, and ethylene glycol—onto the films. In this paper, we discuss the phenomena occurring through conductivities, morphologies, and chemical properties of the modified PEDOT-PSS films as determined using Raman spectroscopy, a four-point probe, scanning electron microscopy (SEM), atomic force microscopy (AFM), transmission electron microscopy (TEM), and X-ray photoelectron spectroscopy (XPS). The schematic 3D morphological model of directly solvent-modified PEDOT:PSS films is presumed for ITO-free devices. The desirable conductivity enhancements of these materials make them attractive candidates for use as anode materials in ITO-free PSCs.

Introduction

The emerging field of polymer photovoltaics (PPVs) is flourishing because these materials appear to have promising technological applications as a result of their of light weight, high flexibility, and solution-processability.[1–3] The power conversion efficiency (PCE) of PPVs has been improved up to 5% AM 1.5G (Air Mass 1.5Global) based on a blend film composed of poly(3-hexylthiophene) (P3HT) as the donor and [6,6]-phenyl-C_{61}-butyric acid methyl ester (PCBM) as the acceptor;[1,2] additionally, the tandem cells with PCE of more than 6.5% were achieved by all-solution processing.[3] This encouraging progress is advancing such materials toward commercial application, where they may eventually compete with inorganic photovoltaics (PVs). Recently, the PPVs with low band gap (LBG) materials,[4–11] processing into large area,[12,13] long-term stability[14,15] and various transparent anodes[16–34] of devices were also widely investigated. LBG polymers were developed to harvest the solar spectrum efficiently in order to generate more photocurrent. The understanding of the complex interplay in large transporting distance and the chemistry that takes place during degradation and failure of device enable devices for large area and longer lifetime. In terms of transparent conducting materials, the choice of applied anode materials is generally limited to indium tin oxide (ITO), carbon nanotube networks,[16,17] silver gratings, random mesh of silver nanowires[18,19] and poly(3,4-ethylenedioxythiophene):poly(styrene sulfonate) (PEDOT:PSS).[20–34] Unfortunately, the high cost of high-quality ITO and its lack of flexibility can limit the solar energy applications of devices incorporating it as an anode material; the limited supply of indium and the transparency of ITO toward visible light are additional problems. Carbon nanotube network films appear to be a suitable alternative: they can be prepared through solution processing, and they exhibited high conductivity and flexibility.[16,17] Such cells do, however, have their problems. For example, the nature of the transparent single-wall carbon nanotube (SWNT) network films is not always well defined; typically, SWNT films are mixtures of metallic and p-doped nanotubes. In addition, it is necessary to add PEDOT:PSS to adjust the work function of the SWNTs and to avoid shorting of the device by having the metallic nanotubes transport electrons from the PCBM materials to the transparent anode. By using vapor-phase polymerization (VPP), the PPV device with desirable conductivity of VPP-PEDOT-Tos films have been demonstrated by Krebs *et al.*,[28] however this material is not solution processable and the work function (WF) suggested by Lindell *et al.* is suitable for a cathode in PPV device (WF = 4.3 eV).[31] The silver grating or random mesh of silver nanowires systems were promising methods to reduce the sheet resistance as electrodes to apply in PPVs,[18,19] however further coating of PEDOT:PSS was needed to adjust the work function and avoid shorting. In short, the most promising material at present is PEDOT:PSS, but it remains a necessary challenge to improve the conductivity of PEDOT:PSS films up to the level exhibited by ITO. PEDOT:PSS films are already used in most organic optoelectronic devices to flatten the ITO surface and tailor the work function of the anodes for hole collection. PEDOT:PSS suffers, however, from low conductivity, which restricts its use as a true electrode material; the conductivity of commercially available PEDOT:PSS (Baytron P, Bayer Corporation), for example, is *ca.* 1 S cm^{-1}, which is lower than that of ITO by three orders of magnitude.

[a]*Department of Materials Science and Engineering, National Chiao Tung University, Hsinchu 300, Taiwan, ROC. E-mail: wtwhang@mail.nctu.edu.tw; Fax: +886-35-724727; Tel: +886-35-731873*
[b]*Material and Chemical Research Laboratories, Industrial Technology Research Institute, Hsinchu 300, Taiwan, ROC*

The conductivity of PEDOT:PSS films can be enhanced through processing with certain solvents and other compounds.[20,22–28,30–33] Kim *et al.* reported that addition of a high-dielectric solvent, such as dimethyl sulfoxide or *N*,*N*-dimethylformamide,[21] into an aqueous solution of PEDOT:PSS can enhance the conductivity of the resulting PEDOT:PSS films by more than one order of magnitude as a result of weakening of the coulombic attraction between the counter ions and the charge carriers. Sorbitol, ethylene glycol, and other alcohols[20,22–27,30,32–33] comprise another set of inert secondary dopants that enhance the conductivity. Although the exact origin of the conductivity enhancement has not been determined, several mechanisms have been proposed. It is generally believed, however, that the presence of the solvent improves the morphology of the films, providing good percolating paths among the PEDOT-PSS domains (PEDOT-rich regions) and transforming the molecular structure.

Our goal for this study was to develop a simple method for modifying the electrical conductivity of PEDOT:PSS films intended for use as electrodes in ITO-free solar cells. We found that high-conductivity PEDOT:PSS films could be obtained simply through spin-coating of a solvent onto pre-coated PEDOT:PSS films. We employed Raman and UV-Vis spectroscopy, a four-point probe, scanning electron microscopy (SEM), tapping-mode atomic force spectroscopy (AFM), transition electron microscopy (TEM), and X-ray photoelectron spectroscopy (XPS) to determine the origin of the conductivity enhancement. We found that the performance of the PPVs was related to the surface morphologies, chemical structures, and electrical conductivities of the PEDOT:PSS films. We performed a comprehensive investigation of the effects of alcoholic and ethereal solvents, including methoxyethanol, ethanol, and 1,2-dimethoxyethane, to determine the driving force for the conductivity enhancement of the PEDOT:PSS films.

Experimental

A. Materials and polymer solar cells

The high-conductivity PEDOT:PSS anodes were prepared using a two-step method. PEDOT:PSS (Baytron P V4071 from Bayer Corporation) was filtered through a 0.45 μm filter prior to being deposited onto cleaned glass substrates at a thickness of *ca.* 50 nm through spin-coating at 4500 rpm in the air. Surface-modifying solvents, namely ethanol (with one hydroxyl group), methoxyethanol (one hydroxyl and one ether group), 1,2-dimethoxyethane (two ether groups), and ethylene glycol (two hydrozyl groups), were spin-coated onto the pristine PEDOT:PSS films, which were then dried at 150 °C for 1 h inside a glove box. A blend [0.9 : 1 (w/w), 17 mg mL^{-1} in dichlorobenzene (DCB) of [6,6]-phenyl-C61-buytyric acid methyl ester (PCBM) and poly(3-hexylthiophene) (P3HT; Rieke Met. Inc.) was stirred overnight in DCB, filtered through a 0.2-μm poly(tetrafluoroethlene) (PTFE) filter, and then spin-coated (450 rpm, 60 s) on top of the PEDOT:PSS layer. The device was completed by coating 30- and 100-nm-thick layers of Ca and Al, respectively, under pressures of less than 10^{-6} Torr. The cell was then encapsulated using UV-curing glue (Nagase, Japan). The active area of all devices, defined through the shadow mask to limit the area of input light and the selective-area sizes of masks were 0.01 and 0.02 cm^2. Fig. 1 displays the architecture (left side; right side (lower)), photograph (right side (upper)) of ITO-free polymer/fullerene solar cells.

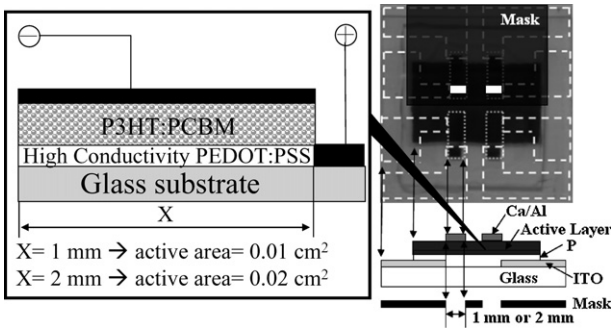

Fig. 1 Architecture and photograph of the ITO-free polymer/fullerene solar cell.

B. Instrumentation

The sheet resistances of the PEDOT:PSS films were measured using a four-point probe; the average of the measured values is reported. The transmittance spectra were recorded using an HP8453 UV-Vis spectrometer. The Raman spectra of the polymer films were recorded using a Renishaw system 2000 micro-Raman system in conjunction with a 632.8-nm HeNe laser as an excitation source. The surface morphologies and phase changes of the PEDOT:PSS films were analyzed using a VEECO DICP-II AFM operated in tapping mode (silicon tips on silicon cantilevers with a spring constant of 2 N m^{-1} and a set point of *ca.* 0.8–0.9) in air. A JEOL JSM-6500F SEM was employed to investigate the thicknesses and morphologies of the PEDOT:PSS films. XPS spectra were recorded using a VG Scientific Microlab 350 spectrometer operated in the constant analyzer energy mode with a pass energy of 50 eV, with MgKα (1253.6 eV) radiation as the excitation source (with normal emission detected). Samples for TEM analysis were prepared through spin-casting of the PEDOT:PSS solution onto the P3HT film (on a glass substrate). The P3HT film was treated with oxygen plasma for 3 min prior to the deposition of PEDOT:PSS. The films were then floated onto THF and placed on a 200-mesh copper TEM grid (Agar Sci., Inc.). The modified PEDOT:PSS films were then prepared according to the procedures described above. TEM images were recorded using a JEOL-2010 TEM and the internal charge-coupled device (CCD) camera. XPS measurements were performed at room temperature and pressures of less than 10^{-10} Torr. Current–voltage (*I*–*V*) curves of the PSC devices were measured using a computer-controlled Keithley 2400 source measurement unit (SMU) equipped with a Peccell solar simulator under the illumination of AM 1.5 (100 mW cm^{-2}). The spectral irradiance data of light source is similar to AM 1.5G solar spectrum (spectral mismatch <5% in the range from 350 to 800 nm). The illumination intensity was calibrated using a standard Si photodiode detector equipped with a KG-5 filter. All of these measurements were performed under an ambient atmosphere at room temperature.

Results and discussion

The origin of conductivity enhancement of surface-modified PEDOT:PSS films

Table 1 lists the sheet resistances of the PEDOT:PSS films, as measured using a four-point probe. The resistance of the pristine PEDOT:PSS (P) film with annealing at 150 °C for 1 h was *ca.* 1011 kΩ cm^{-2}. When the PEDOT:PSS films were modified with ethanol (P-ET), methoxyethanol (P-ME), 1,2-dimethoxyethane (P-DME), and ethylene glycol (P-EG) and then annealed at 150 °C for 1 h under a nitrogen atmosphere, the sheet resistances decreased to 118.6, 7.3, 604.3, and 5.1 kΩ cm^{-2}, respectively. Previous reports of the solvent-doping effect have suggested[20,22–27,30,32–33] that alcoholic solvents enhance the conductivity to a greater extent than ethereal solvents do. We observed conductivity enhancement after the addition of ethanol – in direct contrast to the findings of a previous study, which suggested that alcoholic compounds containing only one hydroxyl group, such as methanol, ethanol, and heptanol, did not enhance the conductivity after they had been added into the aqueous PEDOT:PSS solution.[24,27] We suspect that the boiling point of the additive is an important factor in such solvent-doping systems. For example, a solvent having a low boiling point would evaporate before or with water after spin-coating of the PEDOT:PSS solution; if so, then conductivity enhancement would not be observed. In our approach, however, solvent treatment following film formation would provide solvents with only one OH group, such as ethanol, the opportunity to change the conductivity of the pristine PEDOT:PSS film. The phenomenon of conductivity enhancement of solvent-modified films is discussed in detail below. If transparent electrodes are to be used in photovoltaic devices, they must have high transparency in the visible region of the spectrum. Thicker PEDOT:PSS films will have transmittance and vertical conductivity problems. In this study, a PEDOT:PSS film with thickness of 50 nm was chosen and the transmittance losses of our various solvent-modified PEDOT:PSS films (50 nm thickness) on glass were similar (*ca.* 7%, Table 1).

To determine the mechanism for the conductivity enhancement of the PEDOT:PSS films at the molecular level, we recorded the Raman spectra of the pristine and treated PEDOT:PSS films (Fig. 2). To clearly understand the transformation of the thiophene structures, the presented Raman spectra have been normalized with respect to the intensity of the quinoid peak at 1422 cm^{-1}. The most obvious difference between the pristine and modified PEDOT:PSS films was that the shoulder signal at 1445 cm^{-1} become weaker after solvent modification. The modified films exhibited a narrower band at 1445 cm^{-1}, relative

Table 1 Sheet resistances and transmittances of the PEDOT:PSS films

Anodes	b.p. of modified compound/°C	Sheet resistance/ KΩ cm^{-2}	Transmittance loss at 550 nm (%)
P	none	1011.0 ± 58.5	7.25
P-ET	78	118.6 ± 11.2	7.48
P-ME	124–125	7.3 ± 0.9	7.34
P-DME	85	604.3 ± 126.6	6.34
P-EG	196–198	5.1 ± 1.9	7.36

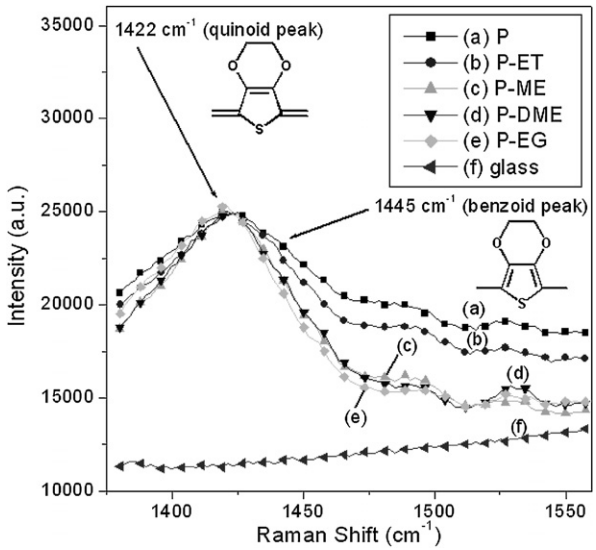

Fig. 2 Raman spectra of PEDOT:PSS films excited using HeNe laser at 632.8 nm.

to the broader band of Yang and co-workers suggested that for P films, the vibrations at 1422 and 1445 cm^{-1} represent to the quinoid and benzoid structures, respectively.[24,27] Our Raman spectra suggest that the conductivity enhancement was due in part to the benzoid structures transforming into quinoid structures. Although the variations of their conductivities were large, the Raman spectra of the P-ME, P-DME and P-EG films were all similar. This finding suggests that the transformation of the thiophene structures was not the only factor enhancing the conductivity of solvent-modified PEDOT:PSS films.

Fig. 4 presents SEM cross-sectional images revealing the thickness and surface topography of the solvent-modified PEDOT:PSS films on glass substrates. Fig. 4(a) indicates that the thickness of the P film was *ca.* 50 nm; its topography was flat and uniform. When the modifying solvent possessed fewer than two hydroxyl groups (*i.e.*, for ET, ME, and DME), the thicknesses and topographies of the films did not change significantly after solvent modification [*cf.* Fig. 4(b)–(d)]. In contrast, EG—a solvent featuring two hydroxyl groups—has a dramatic effect on the thickness and topography of the PEDOT:PSS film [Fig. 4(e)], which became thinner and exhibited a rougher surface morphology. The PEDOT:PSS films generally swell and soften upon the addition of EG.

To investigate if and how any other effect was occurring, we employed AFM in the tapping mode (Fig. 3) to characterize the origin of the conductivity enhancement through measurements of the topographies and phase diagrams of PEDOT:PSS films (0.5 × 0.5 mm^2 area) coated on glass substrates. The phase image of the P film (Fig. 3(A) and 3(B)) was similar to that reported by Crispin *et al.*,[30] with separated PEDOT-PSS domains (PEDOT-rich regions) and PSS domains (PSS-rich regions); the domain sizes and elongated structures were *ca.* 20–30 nm. In the phase image, the hard domains appear as bright regions, which we attribute to PEDOT-PSS domains, whereas the dark regions denote the soft segments that belonged to excess PSS domains.[30] Although the P-ME and P films had similar topographic characteristics, the magnified phase images reveal some variations.

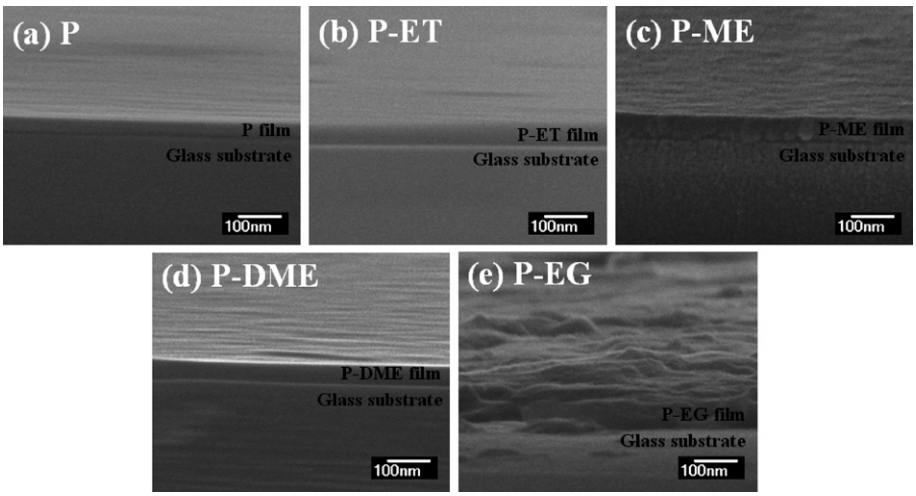

Fig. 3 SEM cross-sectional images of solvent-modified PEDOT-PSS films on glass substrates. (a) P, (b) P-ET, (c) P-ME, (d) P-DME and (e) P-EG.

We observe that ME induced a phase separation that was characterized by segregation of the excess PSS domain surrounded by a continuous PEDOT-PSS phase with higher variation of degree than the P film on phase images. These continuous PEDOT-PSS domains are better percolating pathways that result in higher conductivity. The PEDOT:PSS film had a rougher topography after treatment with EG (Fig. 3(E)), consistent with swelling and softening of the film. The PEDOT-PSS and PSS domains were distinguishable in the phase image with lower variation of degree than the P film on phase images; indeed, the area of the PSS domains (darker regions) underwent an obvious decrease on the polymer surface (Fig. 3(F)). The topographic and phase images reveal that the various solvent treatment processes had quite different effects. In general, the excess PSS domains tended to aggregate, while the PEDOT-PSS domains formed continuous morphologies with the surface phase separation on PEDOT:PSS films.

The ability to observe morphological changes from tapping-mode AFM images is not usually straightforward because the phase image signal is affected by such factors as surface forces, tip indentation, and the bulk properties.[30] To confirm our hypothesis of a correlation existing between the morphology and the conductivity enhancement, we conducted separate TEM experiments using all of the PEDOT:PSS films. The TEM image

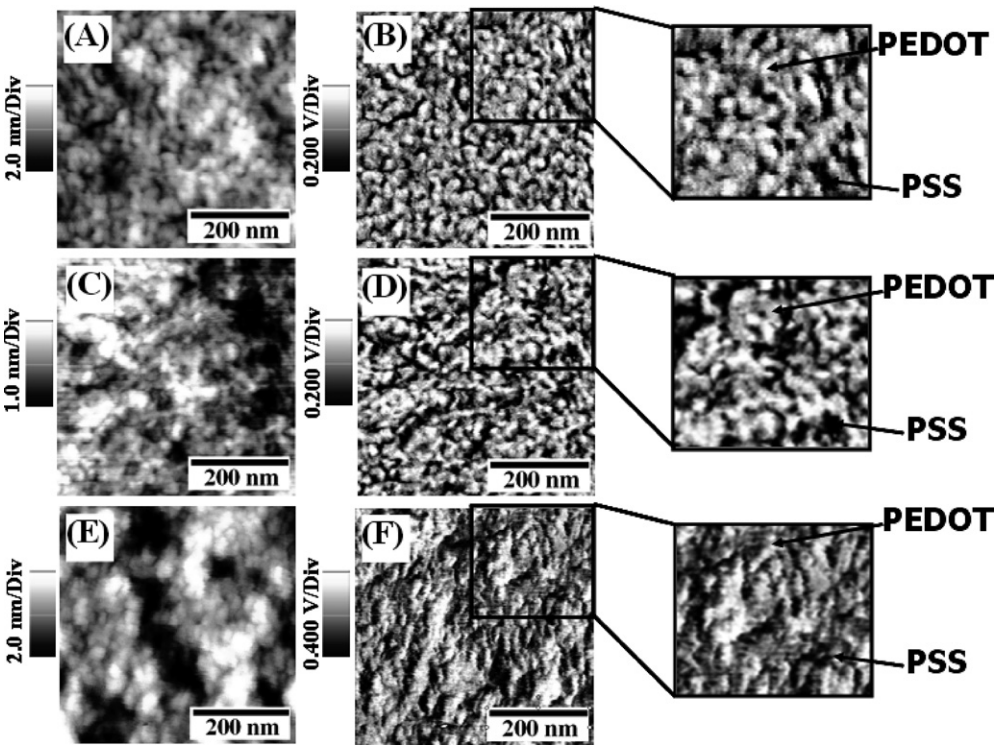

Fig. 4 Topographic (A, C, E) and phase (B, D, F) images of PEDOT-PSS films (P, P-ME and P-EG, respectively) obtained with tapping-mode AFM.

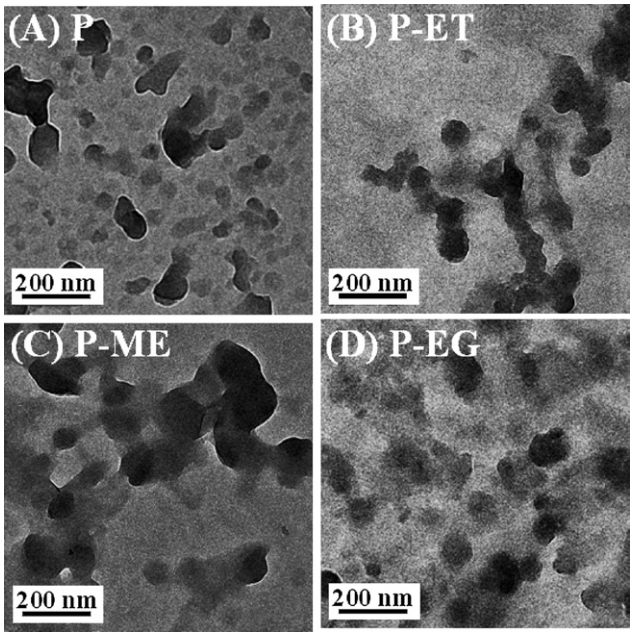

Fig. 5 TEM images of solvent-modified PEDOT-PSS films. (A) P, (B) P-ET, (C) P-ME, and (D) P-EG.

of the P film (Fig. 5(A)) reveals that it consisted of well-defined blends of high-conductivity, darker, isolated PEDOT-PSS domains (PEDOT-rich regions, having grain size *ca.* 50 nm) surrounded by low-conductivity, brighter, excess-PSS domains (PSS-rich regions). In contrast, the TEM images of the P-ET and P-ME films (Fig. 5(B) and 5(C), respectively) reveal indistinct grain boundaries for the conductive PEDOT-PSS domains, having grain sizes *ca.* 80 and 120 nm, respectively. We suspect that the indistinct grain boundaries and the differing grain sizes caused of the variations in the conductivity enhancements; *i.e.*, the P-ME film possessed larger PEDOT-PSS grain sizes and higher conductivity. The grain boundaries of the PEDOT-PSS domains in the P-EG film are difficult to identify in Fig. 5(D) and it is due to the swelling degree of PEDOT-PSS domains is more obviously than P-ME film; thus, the conduction paths of PEDOT-PSS were longer, improving the interconnection of high-conductivity domains within the excess-PSS matrix. Now, through spin-coating with various surface-modified compounds on pristine PEDOT:PSS films, the grain size difference of PEDOT-PSS domains from AFM and TEM can be understood. Taking the P film into account, the inner phase separation of PEDOT-PSS domains can be observed with realer grain size *ca.* 50 nm (from TEM), however, the surface phase separation of PEDOT-PSS domains are having smaller grain size *ca.* 20–30 nm (from AFM) and that is come from detecting the top side of PEDOT-PSS domains. In the P-ME film, the inner phase separation of PEDOT-PSS domains can be observed with realer grain size *ca.* 120 nm (from TEM) and the surface phase separation of PEDOT-PSS domains are more continuously with undistinguished grain size (from AFM).

Although Crispin *et al.* have used XPS measurements (with grazing emission detected) and AFM to completely investigate the phase separation on the surface of PEDOT:PSS films (with and without 5 wt% diethylene glycol),[30] in order to complement the observed morphological changes of PEDOT:PSS layer through spin-coating selective solvents, we performed XPS measurements (with normal emission detected) of these films to determine the inner compositional changes of the surface. Fig. 6–8 display the C(1s), O(1s), and S(2p) core level XPS spectra, respectively. The C(1s) core level spectra of the P films before and after annealing display the same features: a strong peak at 285.0 eV (from C–C or C=C bonds in PEDOT and PSS chains) and a shoulder at 286.5 eV (from C–O–C bonds in PEDOT). We observed similar features for the P-ME and P-EG films; *i.e.*, the insignificant changes in the C(1s) core level features suggested that no chemical changes had occurred. In contrast, when ET and DME were used to modify the PEDOT:PSS films, weak shoulders appeared at 289 eV, corresponding to C=O bonds (Fig. 6(c) and 6(e), respectively). A previous investigation into the over-oxidation of polythiophene suggested that ET and DME (each possessing one OH group) can induce partial decomposition of thiophene moieties, forming C=O bonds.[35]

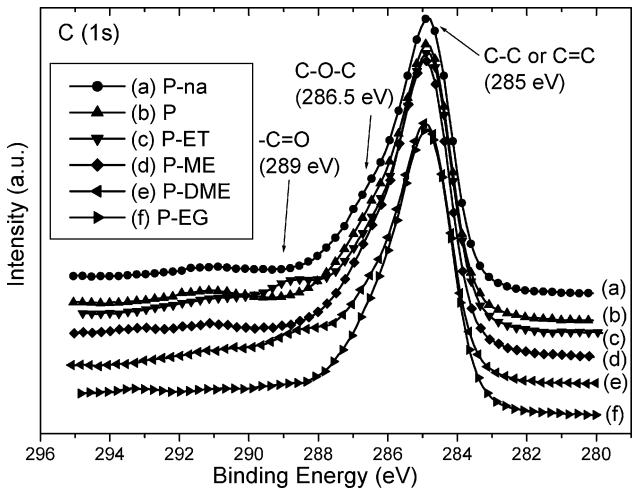

Fig. 6 C(1s) core level spectra before and after heat treatment of (a) P-na, (b) P, (c) P-ET, (d) P-ME, (e) P-DME, and (f) P-EG.

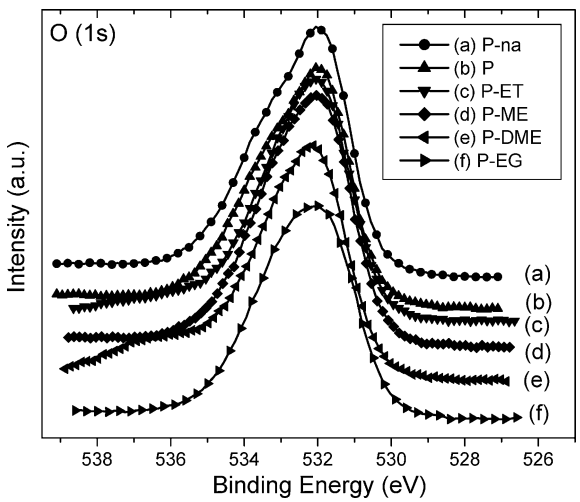

Fig. 7 O(1s) core level spectra before and after heat treatment of (a) P-na, (b) P, (c) P-ET, (d) P-ME, (e) P-DME, and (f) P-EG.

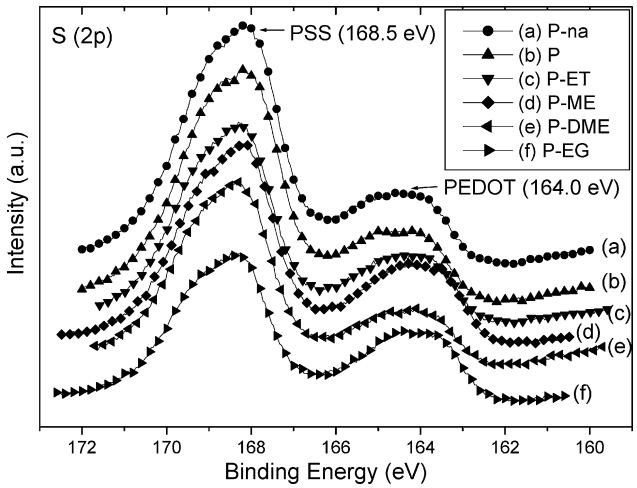

Fig. 8 S(2p) core level spectra before and after heat treatment of (a) P-na, (b) P, (c) P-ET, (d) P-ME, (e) P-DME, and (f) P-EG.

The O(1s) core level XPS spectra of the PEDOT:PSS films in Fig. 7 display a shoulder at *ca.* 533 eV with high binding energy, corresponding to the oxygen atoms of the PEDOT chain, and a strong peak at *ca.* 531 eV with lower binding energy, arising from the SO_3H and $SO_3^-Na^+$ units of the PSS chains.[36] There were no obvious changes in the chemical environments of the oxygen atoms after heat or solvent treatment. The S(2p) core level spectra of PEDOT:PSS films (Fig. 8) exhibited no obviously spin-split peaks from the PSS and PEDOT chains-a result that differs from that reported by Jönsson *et al.*[36] We observe that the PSS chains resulted in a strong peak at *ca.* 168.5 eV, while the PEDOT chains are represented by a strong peak at *ca.* 164 eV. To rationalize the surface changes of the PEDOT and PSS components after treatment with heat and solvent, we used the Shirley method to calculate the peak areas of the S(2p) core level features of the PEDOT and PSS chains. Table 2 indicates that the PEDOT-to-PSS ratios of the pristine and annealed films were similar (0.185–0.187). After solvent modification, the PEDOT-to-PSS ratios of the P-ET and P-DME films were 0.276 and 0.217, respectively, implying that the PSS component had moved away from or was slightly washed out of the surface of the PEDOT:PSS films. After ME and EG were employed as coating solvents, the PEDOT-to-PSS ratios increased to 0.308 and 0.420, respectively. This analysis of the S(2p) core levels reveals that a higher solvent polarity resulted in lower amounts of PSS remaining on the surfaces of the PEDOT:PSS films. As a result, the PEDOT:PSS films treated this way had higher conductivity, which correlated to the PEDOT-to-PSS ratio.

Table 2 Atomic percentages of PEDOT and PSS and PEDOT-to-PSS ratios (from XPS data, calculated using the Shirley method)[ab]

Anodes	At.% of PEDOT	At.% of PSS	PEDOT-to-PSS ratio
P-na	15.63	84.37	0.185
P-a	15.76	84.24	0.187
P-ET-a	21.66	78.34	0.276
P-ME-a	23.52	76.48	0.308
P-DME-a	17.83	82.17	0.217
P-EG-a	29.60	70.40	0.420

[a] na: films with no annealing. [b] a: films with annealing at 150 °C for 1 h.

Timpanaro *et al.* have reported the grain size difference of PEDOT:PSS films through conducting AFM;[37] The separation of pancake-shaped PEDOT-PSS domains by lamellas of PSS have been revealed by Nardes *et al.* through cross-sectional AFM.[38,39] Comparison with previous reports on schematic morphological models of PEDOT:PSS films,[37–39] the schematic 3D morphological model of high-conductivity PEDOT:PSS films could be concluded from SEM, AFM, TEM and XPS analysis in this study (Fig. 9). The information of film thickness and morphology were obtained by SEM images; the AFM measurements revealed the surface phase separation of PEDOT-PSS and PSS domains; TEM images gave the perspective drawing of films with grain size and grain boundary changes. By integrating SEM, TEM and XPS results the swelling property and inner phase separation of films were obtained. The washing out of excess PSS from the surfaces of films could be concluded by comparing AFM phase images and XPS results. As shown in Fig. 9(A)(top-view) and 9(B)(side-view), the morphology of P film were proposed. The pancake-shaped smaller PEDOT-PSS domains (upper layer in P film) and larger PEDOT-PSS domains (lower layer in P film) are separated by continuous PSS domains with obviously grain boundary. In P-ME film (Fig. 9(C) and 9(D)), because ME may slightly diffuse into the PEDOT:PSS film and partial swell the upper layer of PEDOT-PSS domains, the PEDOT-PSS domains (upper layer in P-ME film) would rearrange in the nanophase with larger grain size and partial indistinctly grain boundary. Moreover, when the thickness of P-EG

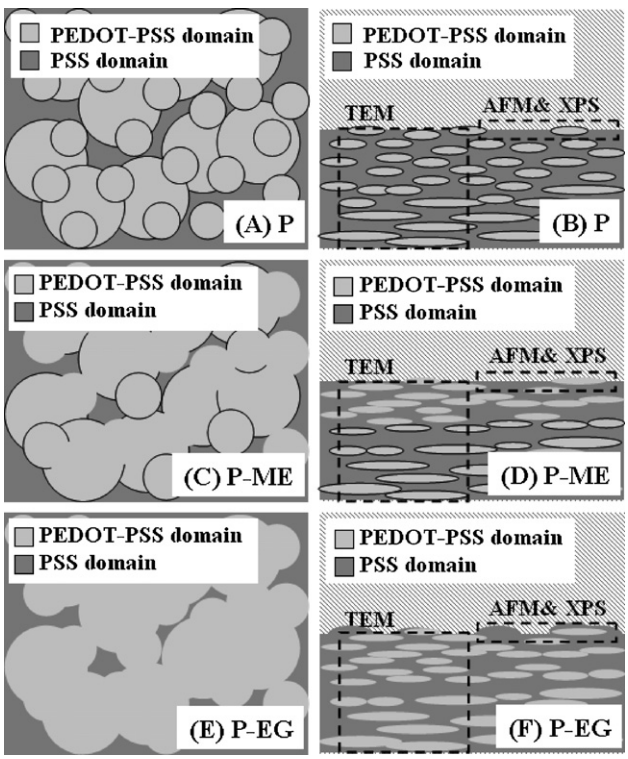

Fig. 9 Schematic 3D morphological models of (A) P (top-view), (B) P (side-view), (C) P-ME (top-view), (D) P-ME (side-view), (E) P-EG (top-view), (F) P-EG (side-view).

film (Fig. 9(E) and 9(F)) is *ca.* 50 nm, the degree of diffusing and swelling effects on P-EG film is apparent that the topography are non-uniform and the PEDOT-PSS domains would form longer conduction paths with indistinctly grain boundary.

Application of solvent-modified PEDOT:PSS film in ITO-free solar cells

Table 3 and Fig. 10 summarize the device performances of ITO-free solar cells incorporating the various PEDOT:PSS films. As expected, the high-conductivity PEDOT:PSS films exhibited improved device efficiency. In general, the power conversion efficiencies (PCEs) of the ITO-free photovoltaic devices were strongly related to the sheet resistances of their PEDOT:PSS films. We observed poor current densities, fill factors, and PCEs for the devices prepared using the P, P-ET, and P-DME films as anodes. When ME and EG were used to modify the films, we obtained higher current densities, fill factors, and efficiencies. The PCEs of the P-ME and P-EG devices were 3.13 and 3.39%, respectively, under AM 1.5G (active layer area: 0.01 cm^2).

Table 3 Performance of PEDOT:PSS/P3HT:PCBM/Ca/Al photovoltaic devices with various active areas under illumination of AM 1.5 (100 mW cm^{-2})

Anode	J_{sc}/mA cm^{-2}	V_{oc}/V	FF	PCE (%)
P[a]	0.79	0.45	0.29	0.10
P-ET[a]	6.74	0.58	0.30	1.16
P-ET[b]	3.11	0.56	0.30	0.52
P-ME[a]	9.50	0.58	0.57	3.13
P-ME[b]	9.10	0.58	0.40	2.11
P-DME[a]	4.32	0.57	0.32	0.78
P-EG[a]	8.99	0.59	0.64	3.39
P-EG[b]	6.75	0.57	0.45	1.72
P/ITO	10.6	0.62	0.58	3.80

[a] Active area of 0.01 cm^2. [b] Active area of 0.02 cm^2. P/ITO: P-coated ITO anodes annealed at 150 °C for 1 h (active area: 0.04 cm^2).

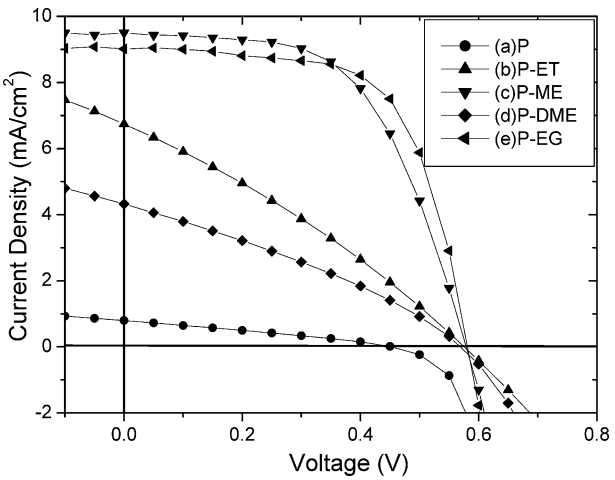

Fig. 10 Current–voltage characteristics of ITO-free polymer solar cells incorporating the various solvent-modified PEDOT:PSS films: (a) P, (b) P-ET, (c) P-ME, (d) P-DME, and (e) P-EG. All devices were measured under illumination of AM 1.5 (100 mW cm^{-2}) with active area of 0.01 cm^2.

Table 3 also lists the performance behavior of P-EG and P-ME devices having larger active layer areas (0.02 cm^2). The P-ET device having a small active layer area exhibited an AM 1.5G PCE of 1.16%, with an open-circuit voltage (V_{oc}) of 0.58 V, a short-circuit current density (J_{sc}) of 6.74 mA cm^{-2}, and a fill factor (FF) of 30%. Poorer performance resulted from using a larger-area active layer, with the values of the FF, J_{sc}, and PCE all decreasing significantly. We observed similar phenomena for the P-ME and P-EG systems: the small and large P-ME devices had PCEs of 3.13 and 2.11%, respectively, while the PCE of the P-EG device decreased from 3.39 to 1.72% upon increasing the area of the active layer. Table 3 also lists the output characteristics of the device employing an ITO glass substrate as the anode and a 50-nm-thick P film as a buffer layer. The performance of P3HT was comparable with that reported previously,[1–3] with the optimum efficiency being *ca.* 3.9%. The devices containing small active areas (0.01 cm^2) of P-ME and P-EG exhibited similar performance in terms of their PCEs relative to that of the device based on ITO. In contrast, the performances of large-active-area (0.02 cm^2) devices were poor for all of the solvent-modified systems. Even though the electrical conductivity was dramatically enhanced through ME- and EG-modification, there is obviously a distance effect for PEDOT:PSS based ITO-free PPV devices (Fig. 1). When using the large-active-area device, the increasing sheet resistance *via* PEDOT:PSS layer to electrode is observed to decrease J_{sc}.

Conclusions

We have employed Raman and UV-Vis spectroscopy, SEM, tapping-mode AFM, TEM, and XPS to investigate the origin of the sheet resistance decrease of solvent-modified PEDOT:PSS films. The spin-coating of directly solvent-modified PEDOT:PSS films led to transformation of the chemical structure of PEDOT (from Raman spectroscopic analysis), phase segregation of PEDOT-PSS and PSS domains (from SEM, AFM, TEM and XPS analyses), and washing out excess PSS from the surfaces of the PEDOT:PSS films (from XPS analysis). From a comparison of the variation in conductivity of the modified films, we conclude that phase segregation enabled the formation of longer conduction paths of PEDOT-PSS domains. This phenomenon was the major influence on the conductivity enhancement; the transformation of the PEDOT structure and the decrease in the content of PSS domains on the polymer surface were secondary effects. ITO-free solar cells fabricated using these high-conductivity PEDOT:PSS films as anodes exhibit a high performance. The PCEs of the solar cell devices incorporating ME- and EG-modified PEDOT:PSS films reached 3.13 and 3.39%, respectively, under illumination of AM 1.5 (100 mW cm^{-2}).

Acknowledgements

We thank the National Science Council (project NSC 96-2221-E-009-015) and the Ministry of Economic Affairs, Taiwan, for financial support.

References

1 G. Li, V. Shrotriya, J. S. Huang, Y. Yao, T. Moriarty, K. Emery and Y. Yang, *Nat. Mater.*, 2005, **4**, 864.

2 W. L. Ma, C. Y. Yang, X. Gong, K. Lee and A. J. Heeger, *Adv. Funct. Mater.*, 2005, **15**, 1617.
3 J. Y. Kim, K. Lee, N. E. Coates, D. Moses, T.-Q. Nguyen, M. Dante and A. J. Heeger, *Science*, 2007, **317**, 222.
4 C. J. Brabec, N. S. Sariciftci and J. C. Hummelen, *Adv. Funct. Mater.*, 2001, **11**, 15.
5 H. Spanggaard and F. C. Krebs, *Sol. Energy Mater. Sol. Cells*, 2004, **83**, 125.
6 K. M. Coakley and M. D. McGehee, *Chem. Mater.*, 2004, **16**, 4533.
7 H. Hoppe and N. S. Sariciftci, *J. Mater. Res.*, 2004, **19**, 1924.
8 E. Bundgaard and F. C. Krebs, *Sol. Energy Mater. Sol. Cells*, 2007, **91**, 954.
9 S. Günes, H. Neugebauer and N. S. Sariciftci, *Chem. Rev.*, 2007, **107**, 1324.
10 M. Jorgensen, K. Norrman and F. C. Krebs, *Sol. Energy Mater. Sol. Cells*, 2008, **92**, 686.
11 B. C. Thompson and J. M. J. Fréchet, *Angew. Chem., Int. Ed.*, 2008, **47**, 58.
12 F. C. Krebs, H. Spanggard, T. Kjær, M. Biancardo and J. Alstrup, *Mater. Sci. Eng. B*, 2007, **138**, 106.
13 C. Lungenschmied, G. Dennler, H. Neugebauer, S. N. Sariciftci, M. Glatthaar, T. Meyer and A. Meyer, *Sol. Energy Mater. Sol. Cells*, 2007, **91**, 379.
14 X. Yang, J. Loos, S. C. Veenstra, W. J. H. Verhees, M. M. Wienk, J. M. Kroon, M. A. J. Michels and R. A. J. Janssen, *Nano Lett.*, 2005, **5**, 579.
15 F. C. Krebs and K. Norrman, *Prog. Photovolt, Res. Appl.*, 2007, **15**, 697.
16 M. W. Rowell, M. A. Topinka, M. D. McGehee, H. J. Prall, G. Dennler, N. S. Sariciftci, L. Hu and G. Gruner, *Appl. Phys. Lett.*, 2006, **88**, 233506.
17 A. D. Pasquier, H. E. Unalan, A. Kanwal, S. Miller and M. Chhowalla, *Appl. Phys. Lett.*, 2005, **87**, 203511.
18 T. Aernouts, P. Vanlaeke, W. Geens, J. Poortmans, P. Heremans, S. Borghs, R. Mertens, R. Andriessen and L. Leenders, *Thin Solid Films*, 2004, **451**, 22.
19 J. Y. Lee, S. T. Connor, Y. Cui and P. Peumans, *Nano Lett.*, 2008, **8**, 689.
20 F. Zhang, M. Johansson, M. R. Andersson, J. C. Hummelen and O. Inganäs, *Adv. Mater.*, 2002, **14**, 662.
21 J. Y. Kim, J. H. Jung, D. E. Lee and J. Joo, *Synth. Met.*, 2002, **126**, 311.
22 B. D. Martin, N. Nikolov, S. K. Pollack, A. Saprigin, R. Shashidhar, F. Zhang and P. A. Heiney, *Synth. Met.*, 2004, **142**, 187.
23 Y. H. Ha, N. Nikolov, S. K. Pollack, J. Mastrangelo, B. D. Martin and R. Shashidhar, *Adv. Funct. Mater.*, 2004, **14**, 615.
24 J. Ouyang, Q. Xu, C. W. Chu, Y. Yang, G. Li and J. Shinar, *Polymer*, 2004, **45**, 8443.
25 S. Ashizawa, R. Horikawa and H. Okuzaki, *Synth. Met.*, 2005, **153**, 5.
26 J. Hung, P. F. Miller, J. S. Wilson, A. J. de Mello, J. C. de Mello and D. D. C. Bradley, *Adv. Funct. Mater.*, 2005, **15**, 290.
27 J. Ouyang, C. W. Chu, F. C. Chen, Q. Xu and Y. Yang, *Adv. Funct. Mater.*, 2005, **15**, 203.
28 B. Winther-Jensen and F. C. Krebs, *Sol. Energy Mater. Sol. Cells*, 2006, **90**, 123.
29 J. Huang, X. Wang, Y. Kim, A. J. de Mello, D. D. C. Bradley and J. C. de Mello, *Phys. Chem. Chem. Phys.*, 2006, **8**, 3904.
30 X. Crispin, F. L. E. Jakobsson, A. Crispin, P. C. M. Grim, P. Andersson, A. Volodin, C. van Haesendonck, M. van der Auweraer, W. R. Salaneck and M. Berggren, *Chem. Mater.*, 2006, **18**, 4354.
31 L. Lindell, A. Burquel, F. L. E. Jakobsson, V. Lemaur, M. Berggren, R. Lazzaroni, J. Cornil, W. R. Salaneck and X. Crispin, *Chem. Mater.*, 2006, **18**, 4246.
32 T. Y. Kim, J. E. Kim and K. S. Suh, *Polym. Int.*, 2006, **55**, 80.
33 C. J. Ko, Y. K. Lin, F. C. Chen and C. W. Chu, *Appl. Phys. Lett.*, 2007, **90**, 063509.
34 S. Chaudhary, H. Lu, A. M. Müller, C. J. Bardeen and M. Ozkan, *Nano Lett.*, 2007, **7**, 1973.
35 U. Barsch and F. Beck, *Electrochim. Acta*, 1996, **41**, 1761.
36 S. K. M. Jönsson, J. Brigerson, X. Crispin, G. Greczynski, W. Osikowicz, A. W. Denier van der Gon, W. R. Salaneck and M. Fahlman, *Synth. Met.*, 2003, **10361**, 1.
37 S. Timpanaro, M. Kemerink, F. J. Touwslarger, M. M. de Kok and S. Schrader, *Chem. Phys. Lett.*, 2004, **394**, 339.
38 A. M. Nardes, M. Kemerink, R. A. J. Janssen, J. A. M. Bastiaasen, N. M. M. Kiggen, B. M. W. Langeveld, A. J. J. M. van Breemen and M. M. de Kok, *Adv. Mater.*, 2007, **19**, 1196.
39 A. M. Nardes, M. Kemerink and R. A. J. Janssen, *Phys. Rev. B*, 2007, **76**, 085208.